Nanotube-Bridged Wires with Sub-10 nm Gaps

ARTICLE *in* NANO LETTERS · MARCH 2012

Impact Factor: 13.59 · DOI: 10.1021/nl204259t · Source: PubMed

NANO LETTERS

Letter

pubs.acs.org/NanoLett

Nanotube-Bridged Wires with Sub-10 nm Gaps

Byung Yang Lee,[†,#] Kwang Heo,[‡,#] Abrin L. Schmucker,[§] Hye Jun Jin,[†] Jong Kuk Lim,[⊥] Taekyeong Kim,[†] Haemi Lee,[∥] Ki-Seok Jeon,[∥] Yung Doug Suh,[∥] Chad A. Mirkin,*[,§] and Seunghun Hong*[,†,‡,§]

[†]Department of Physics and Astronomy, [‡]Interdisciplinary Program in Nano-Science and Technology, and [§]Department of Biophysics and Chemical Biology (WCU Program), Seoul National University, Seoul 151-747, Korea

[§]Department of Chemistry, Northwestern University, Evanston, Illinois 60208-3113, United States

[⊥]Department of Chemistry, Chosun University, Gwangju 501-759, Korea

[∥]Laboratory for Advanced Molecular Probing (LAMP), NanoBio Fusion Research Center, Korea Research Institute of Chemical Technology, Daejeon, 305-600, Korea

S *Supporting Information*

ABSTRACT: We report a simple but efficient method to synthesize carbon nanotube-bridged wires (NBWs) with gaps as small as 5 nm. In this method, we have combined a strategy for assembling carbon nanotubes (CNTs) inside anodized aluminum oxide pores and the on-wire lithography technique to fabricate CNT-bridged wires with gap sizes deliberately tailored over the 5−600 nm range. As a proof-of-concept demonstration of the utility of this architecture, we have prepared NBW-based chemical and biosensors which exhibit higher analyte sensitivity (lower limits of detection) than those based on planar CNT networks. This observation is attributed to a greater surface-to-volume ratio of CNTs in the NBWs than those in the planar CNT devices. Because of the ease of synthesis and high yield of NBWs, this technique may enable the further incorporation of CNT-based architectures into various nanoelectronic and sensor platforms.

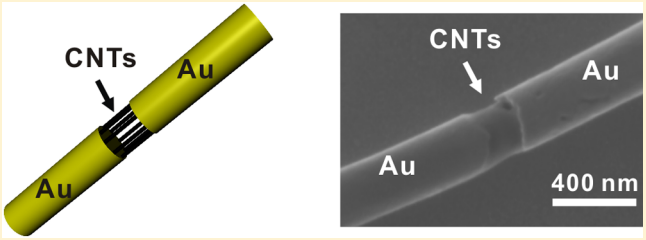

KEYWORDS: *Carbon nanotube, nanowire, transducer, on-wire lithography, template-directed synthesis*

Carbon nanotubes (CNTs) have been utilized for a wide variety of advanced devices due to their remarkable electronic properties.[1] For certain device applications, it is often advantageous to use a short CNT channel.[2,3] For example, CNT channels with sub-10 nm lengths can exhibit ballistic electron transport and have been utilized as active components for various devices, such as transistors,[4] interconnectors,[5] biosensors,[6,7] and actuators.[8] Some of the methods to produce CNT devices with sub-10 nm channels include procedures based upon conventional nanolithography methods, such as e-beam lithography,[3] focused-ion beam (FIB),[9] and angled metal deposition.[2] However, these methods often require time-consuming and complicated processing steps.

Recently, on-wire lithography (OWL) has been developed as a technique to synthesize billions of gapped nanowires (GNWs) with nanometer control of gap length, within a single experiment.[10−12] The fine control of geometry, composition, and placement along the linear array afforded by OWL has enabled a variety of investigations in the fields of plasmonics, surface-enhanced Raman spectroscopy, surface plasmon-mediated energy transfer, and nanoencoding.[13−17] Additionally, these architectures have been utilized as a test bed for molecular transport junctions (MTJs) by fabricating sub-10 nm gaps between Au electrodes that are bridged by molecular wires.[18−20] Because of OWL's ability to precisely control the dimensions of nanogaps with nanometer precision, OWL-synthesized structures represent ideal nanoarchitectures for investigating the fundamental properties of sub-10 nm CNT channels, which may then be utilized in future work to fabricate large arrays of functional devices. Herein, we report a simple but efficient method to produce nanotube-bridged wires (NBWs) including CNT channels with channel lengths as small as 5 nm by combining two techniques: assembling CNTs inside anodized aluminum oxide (AAO) pores and the OWL method.[10,21]

In a typical experiment, the CNTs were first assembled on the sidewalls of pores in AAO (Anodisk, Whatman Inc., USA) substrates (Figure 1a,b). The diameter of the pores was 360 ± 20 nm, which determined the diameter of our NBW structures. Because CNTs are known to assemble onto Al and Al_2O_3 surfaces,[22,23] the CNTs were able to assemble onto the sidewalls of the AAO, while the aqueous solution containing the surfactant (SDS)-stabilized CNTs was passed through the pores. Then, a 400 nm-thick Ag layer was thermally deposited on one side of the AAO template to serve as a working electrode for the subsequent electrodeposition of the metals required to implement the OWL process (Figure 1c). After

Received: December 3, 2011
Revised: March 6, 2012
Published: March 23, 2012

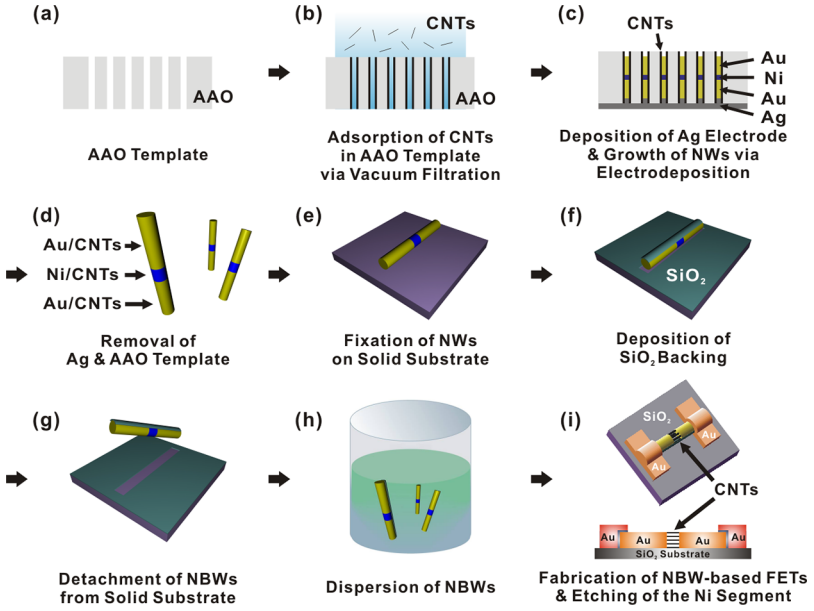

Figure 1. Schematic diagram depicting the fabrication process of NBWs with sub-5 nm-long CNT channels. (a) AAO template. (b) Adsorption of CNTs on the sidewalls of the pores in the AAO template via vacuum filtration. (c) Deposition of Ag electrode and growth of NWs with the segments of Au and Ni via the electrodeposition method. (d) Removal of the AAO template. (e) Fixation of NWs on solid substrate. (f) Deposition of SiO_2 backing. (g) Detachment of the silicate-backed NBWs. (h) Dispersion of the silicate-backed NBWs. (i) Fabrication of NBW-based FETs and etching of the Ni segment.

thermal Ag deposition, additional Ag was electrochemically deposited using a potentiostat (reference 600, Gamry Instruments Inc.) to create a uniform working electrode for the deposition of the first Au segments. In this process, a platinum (Pt) counter electrode and an Ag/AgCl reference electrode were used for the electrodeposition process. The desired Au, Ni, and Au segments were then electrodeposited in series.[21] Nanowire structures were formed because the AAO template allowed the metal to be deposited along the long axis of the pore while maintaining a consistent nanowire diameter. The lengths of the Ni and Au segments were controlled by the total amount of charge passed through the electrochemical cell.[11] Following the deposition, the Ag layer was removed with an etching solution consisting of methanol, 30% ammonium hydroxide, and 30% hydrogen peroxide (4:1:1 v/v/v)[24] (Figure 1d). The AAO template was then dissolved in an aqueous solution of 3 M NaOH and rinsed thoroughly with deionized (D.I.) water and ethanol. The NWs were then cast on a solid glass substrate (Figure 1e), and a 50 nm thick silica (SiO_2) backing was deposited using plasma-enhanced chemical vapor deposition (PECVD) (Figure 1f). Following the deposition of the backing layer, the NWs were then detached from the glass substrate via sonication and dispersed in D.I. water (Figure 1g,h). After a single fabrication process, we were able to obtain $\sim 10^9$ or more nanowires with the electrochemically programmed Au−Ni−Au architecture. Finally, the NWs were cast on a SiO_2 substrate where source and drain metal electrodes were fabricated on each side of the NW via e-beam lithography (Figure 1i). Importantly, this remains the rate limiting step in device fabrication, as individual NBWs must be addressed to connect to larger contact electrodes. NBW-based field effect transistors (FETs) were made by etching the Ni segments in a 1 M aqueous $FeCl_3$ solution to form CNT channels between the Au segments.[25] The substrate was then washed several times with D.I. water to remove $FeCl_3$, which was followed by further successive rinsing with ethanol and isopropyl alcohol. Finally, isopropyl alcohol was evaporated by a critical point dryer.

SEM images of NBWs were taken before and after (Figure 2a, left and right, respectively) the etching of the Ni segments. The relatively dark area in the middle of the NBW in Figure 2a, left, corresponds to the Ni segment. After removing the Ni segment, the CNTs in the channel region appear to move slightly toward the center of the gap (Figure 2a, right), which is likely due to the absence of the supporting Ni segment. The formation of NBWs with sub-5 nm-long CNT channels was verified by TEM (Figure 2b). The CNT channel length between two Au electrodes (dark area) was 5 nm. Importantly, during the synthesis of these structures, CNTs are likely both on the surface of and embedded within the nanowires. Within a single individual wire, multiple CNT junctions can be fabricated using this novel approach (Figure 2c and Figure S1, Supporting Information). For example, in a proof-of-concept experiment, three Ni segments were electrochemically deposited with 1, 2, and 4 coulombs of charge, giving rise to channel lengths of 150, 300, and 600 nm, respectively. This result shows that we can control the number and the length of CNT channels in NBWs simply by controlling the lengths of the Ni segments during the electrodeposition process. Energy dispersive X-ray spectroscopy (EDX) was subsequently performed on three different wires to confirm the absence of Ni in the CNT channel, and the results were consistent. Before chemically etching the Ni segments, two prominent Ni peaks were visible (Figure 2d). After etching with 1 M $FeCl_3$, these peaks disappeared (Figure 2e). Initially, Au peaks are observed in the gap regions because the electron beam spot size for the EDX measurement was larger than the gap size. Thus, the Au peak came from the Au segment near the gap. Subsequent experiments using NBWs with a rather large gap size of 600 nm did not show any Au peak in the gap region (Figure S2, Supporting Information).

Atomic force microscope (AFM)-coupled Raman spectroscopy[26] was used to characterize the NBWs (Figure 3a). In this

dx.doi.org/10.1021/nl204259t | *Nano Lett.* 2012, 12, 1879−1884

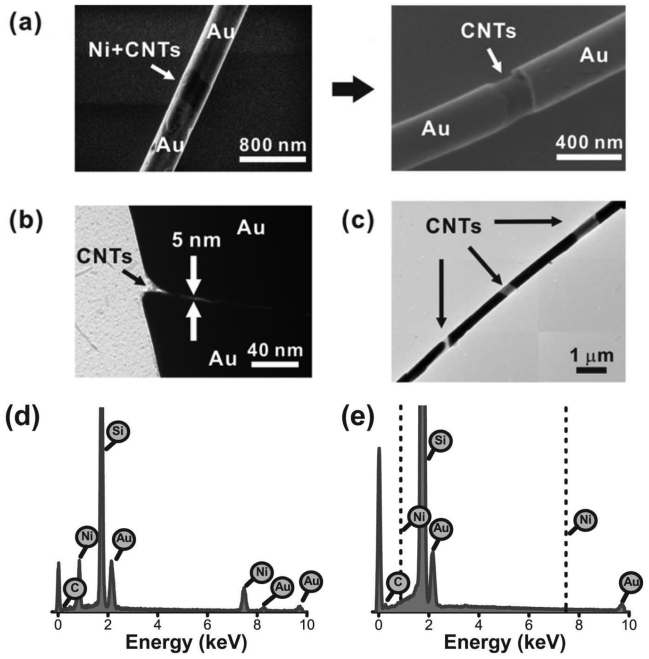

Figure 2. Electron microscopy of NBWs. (a) SEM images of a NBW before (left) and after (right) the removal of the Ni segment. (b) TEM image of a NBW with a 5 nm-long CNT channel. (c) TEM image of a NBW with multiple CNT junctions. Within this image, the four black regions and three gray regions represent Au electrodes and CNT channels, respectively. Two images taken separately are patched to show all three segments in the NBW. (d) EDX spectrum on representative nanowire taken before etching Ni segment. (e) EDX spectrum on representative nanowire after etching the Ni segments. The original locations of Ni peaks have been marked by dotted lines for clarity.

experiment, Raman spectra were recorded using an AFM-correlated nano-Raman microscope equipped with an inverted optical microscope and a piezoelectric *x*, *y* sample scanner manipulated by an independent scanning controller. The 633 nm line of a He−Ne laser was used as the excitation source coupled with a single-mode optical fiber. The tapping-mode closed-loop AFM scanner on top of the closed-loop piezoelectric flexure sample stage was used to correlate the Raman or Rayleigh scattering signal with the AFM topographical image. The laser spot was focused on the center of the AFM tip so that it scattered symmetrically off the apex of the AFM tip.[27] The AFM topographical image of the NBWs with a sub-5 nm-long CNT channel (Figure 3a,i) was correlated with the Raman signal (Figure 3a,ii) with an overlap precision of ∼10 nm. Specifically, the Raman spectrum of a NBW was measured at two different points along the Au wire (P1 and P2) and one channel region (P3). Significantly, G- and D-band peaks were observed at all three regions (Figure 3a,ii). Note that the G- and D-band peak intensities at the CNT channel region (P3) were higher than those at the Au electrode regions (P1 and P2). Presumably, the lattice vibration of the CNTs buried in the Au part of the NW was inhibited, while that of the CNTs in the channel region was not affected because the CNTs were suspended in air.[28,29] Furthermore, we repeated the experiments three times and obtained similar results. We repeated the same measurement on NBWs with a gap size of 600 nm. In this case, we obtained similar Raman measurement results, and the AFM topographical image clearly shows the gap region (Figure S3, Supporting Information).

The electrical properties of the NBW-based FET were studied before (Figure 3b,i) and after (Figure 3b,ii) Ni etching using a Keithley 4200 semiconductor parametric analyzer. Before removing the Ni segment, the NBW-based FET showed typical metallic behavior. However, after etching the Ni segment, the device exhibited nonlinear *IV* characteristics, consistent with the formation of the channels with suspended CNTs (compare Figure 3b,i and 3b,ii). The nonlinear behavior of the NBW-based FET is due to the formation of a Schottky barrier at the interface between the CNT and Au. We measured the electrical properties of multiple devices and obtained consistent results. For example, the NBW-based FETs with a gap size of ∼50 nm exhibited an average conductance value of $\sim 3.4 \times 10^{-5}$ S with a rather uniform distribution similar to that of previously reported devices based on multiple CNTs (Figure S4 in Supporting Information).[22] From the conductance data of our NBW-based FETs and previously reported resistivity values of individual suspended CNTs, we can estimate the number of CNTs which bridged the gap. For example, in our NBW structure with a gap distance of 50 nm, the gap was connected by multiple CNTs with a diameter of ∼2 nm. Previous work shows that the resistivity of a suspended semiconducting or metallic CNT is $\sim 0.8 \times 10^{-4}$ or $\sim 1.1 \times 10^{-5}$ Ω·m, respectively.[30,31] Since we utilized unsorted CNTs, we can assume that the gap of the NBW was connected by a group of CNTs with its semiconducting and metallic CNT composition of 2:1 just like as-grown CNT powders. As a result, we could estimate that the gap of our NBW with a diameter of ∼360 nm was connected by ∼11 CNTs.

Figure 3c shows the current normalized power spectral density S/I^2 of the NBW based FET, where S and I are power spectral density and current, respectively. The noise characteristics of the devices were studied by applying a low-noise dc bias and observing a current spectral density by a fast Fourier transform (FFT) analyzer (SR770, Stanford Research Systems, USA). The graph was fitted with $1/f^{\nu}$ with a fitting scaling parameter ν ∼0.976 (R^2 = 0.9906). This analysis demonstrates that our NBW-based FETs follow a $1/f$ noise characteristic and exhibit a noise amplitude-to-resistance ratio $(A/R) = 7.66 \times 10^{-10}$. This value is comparable to that of previously reported CNT-network devices which typically show A/R values around $\sim 10^{-11}$.[32]

Low-bias resistance values were determined for CNT channels of 150, 300, and 600 nm in length respectively, using a two probe method for testing of similar architectures[18] (Figure 3d). A NBW-based FET with the three CNT junctions was fabricated by forming electrodes on each Au segments of the NBW, including three CNT junctions via e-beam lithography. The size ratio of the three channels was 1:2:4, which results in a resistance ratio of 1:2:4. Based on these data, one can conclude that these structures exhibit diffusive electrical transport characteristics in agreement with those reported previously.[33,34]

This novel platform is ideally suited for making and studying CNT-based chemical and biological sensors. As proof-of-concept, a NBW-based FET with a 50 nm channel length was measured to test its response to external electric fields. The device showed little dependence on the back-gate field, since most of the CNTs in the channel were suspended in air and formed a cylindrical sheet away from the back-gate field. Therefore, we applied a liquid gate bias using a Pt pseudoreference electrode in 100 μM NaCl solution, while the V_{ds} was kept at 0.1 V. When the gate voltage was swept

dx.doi.org/10.1021/nl204259t | *Nano Lett.* 2012, 12, 1879−1884

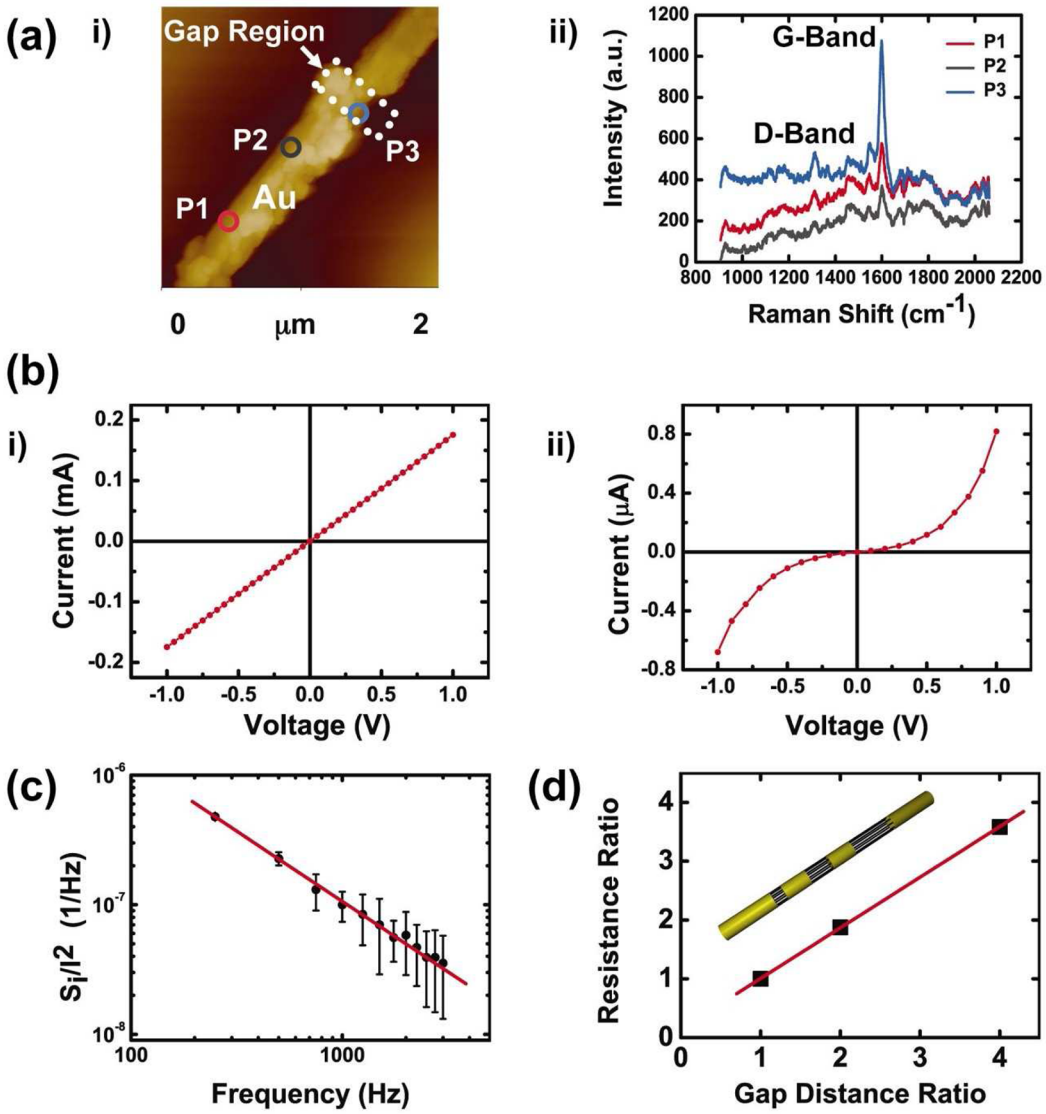

Figure 3. Electronic and optical characterization of NBW-based FETs. (a) AFM-correlated nano-Raman spectroscopic measurements of a NBW. Raman spectroscopy (ii) was performed on the locations of P1, P2, and P3 marked in the AFM image (i) using a 633 nm wavelength laser light with its spot size of 300 nm. (b) *IV* characteristics of the NBW-based FET (i) before and (ii) after the removal of the Ni segment. (c) Noise characteristics of the NBW-based FET. The device exhibited a typical $1/f$ noise behavior and a noise amplitude-to-resistance ratio $A/R \sim 7.66 \times 10^{-10}$. (d) Graph of the resistance versus gap distance of the NBW-based FET with multiple CNT junctions. The resistance of CNT junctions increased linearly as the gap distance increased and measurements were taken at points along a single nanowire.

from −0.4 to 0.4 V, the device showed an on/off ratio of 2 with a typical hysteresis curve (Figure 4a).[22] This dependence shows that the CNT channels in the NBW-based FETs are sensitive to subtle variations in external electric fields. It also suggests that the NBW-based FET can be utilized for chemical sensing.

To test this hypothesis, a NBW-based FET with a 50 nm channel length was synthesized and exposed to NO_2 gas. In this experiment, the resistance of the devices in a gas chamber was monitored at room temperature, while NO_2 gas at different concentrations (0.5, 1, 2, 5, 10 ppm) in N_2 was flowed successively over the device. In agreement with previous reports,[35] the conductance of the CNT channels in the NBW-based FETs increased by the exposure to NO_2. The responses of a NBW-based FET and a planar CNT network-based FET are then compared (Figure 4b). The NBW-based FET current was highly dependent on the exposure to NO_2 gas (Figure 4b, insert). When compared to our results using planar CNT network devices fabricated by the previously reported surface programmed assembly method,[36] (Figure S5, Supporting Information) the NBW-based FET with CNT channels exhibited ~3 times higher sensitivity. The improved sensitivity of the NBW-based FETs can be attributed, in part, to the increased surface-to-volume ratio of the suspended CNTs in the NBW-based FETs. This increase in surface area of CNTs with a finite volume could be advantageous for NO_2 sensing because an increased amount of NO_2 is capable of being absorbed on the exposed surface of the suspended CNTs. Based on these results, it can be concluded that the sensitivity of NBW-based FETs was higher than that of planar CNT-network devices of comparable architecture.

Finally, we utilized this 50 nm channel length architecture for proof-of-concept real-time DNA sensing (Figure 4c). Here, the Au electrodes in NBW-based FETs were functionalized with the thiolated DNA (SH-C_6-5′-GCCACAAACACCA-CAAGA-

dx.doi.org/10.1021/nl204259t | *Nano Lett.* 2012, 12, 1879–1884

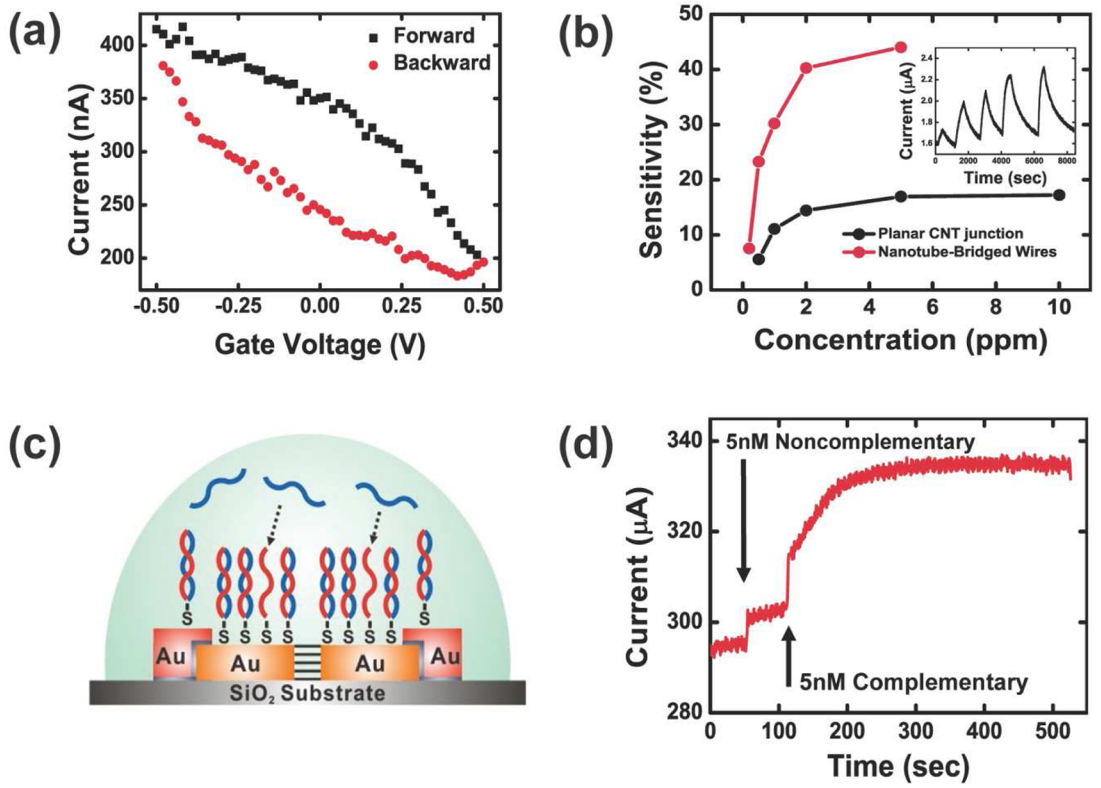

Figure 4. Gating effect measurement and sensing experiment using NBW-based FETs. (a) Liquid gate profile with a typical hysteresis curve. The drain−source voltage was V_{ds} = 0.1 V, and a Pt reference electrode was used. (b) Sensitivity dependence on the concentration of NO_2 gas in the NBW-based FET and planar CNT-network devices. The NBW-based FET showed a higher sensitivity than planar CNT-network devices. The inset shows the real-time response of the NBW-based FET to NO_2 gas. (c) Schematic diagram showing the DNA sensing experiment using the NBW-based FET functionalized with thiolated DNA (SH-C_6-5′-GCCACAAACACCACAAGA-3′) and (d) the real-time response of the NBW-based FET to the injection of non-cDNA or cDNA molecules.

3′) by dipping the NBW-based FETs in the DNA solution (100 nM DNA in D.I. water) for 6 h. Then, 10 mM mercaptohexanol was introduced to create adsorbed spacer molecules. Conductance measurements were performed in ac mode (0.5 V_{rms}, 10 kHz) with the dc bias set to 0 V. The signal was amplified with a current gain preamplifier and detected using a lock-in amplifier. Upon injection of 5 nM non-cDNA sequences (5′-TGGTGGATCCGTTCGCTG-3′), the sensor showed little increase in current (Figure 4d). However, when 5 nM cDNA sequences (5′-CGGTGTTTGTGGTGTTCT-3′) were injected, the real-time sensing signal was ∼5 times higher than that induced by the injection of the noncomplementary segments at the same concentration. The rapid conductance increase by injecting cDNA segments can be explained by the work function modulation of Au electrodes caused by adsorbed DNA molecules on the electrode. In this case, negatively charged cDNA hybridized with the DNA backbone at the electrode surface and induced positively charges on the Au electrodes. This modulation of the work function of the Au electrodes lowered the Schottky barriers between the CNTs and the Au electrodes.[7] The slight conductance increase by injecting non-cDNA fragments can be attributed to an increase of the dielectric constant of the solution by the injection. This result shows that our NBWs can be used as a sensing component in biosensors for detecting specific biomolecules. The sensitivity of the NBW-based sensors is expected to be improved by optimizing various parameters in the future, and would need to be, before being competitive with state of the art DNA detection systems.[37−40] In particular, previous reports show that NO_2 sensors or Schottky-barrier sensors based on a larger number of CNTs exhibited a higher sensitivity.[41−43] Since the number of CNTs in our NBWs depends on the NBW diameter, one might be able to improve the sensor sensitivity by adjusting the diameter of the NBW used for the sensors.

In summary, we report a simple but efficient method to mass produce NBWs, including CNT channels with channel lengths as small as 5 nm. This method allows one to fabricate NBWs, including single or multiple CNT channels with controlled lengths. Optical and electrical characterization results show that the CNT channels embedded in the NBW maintain their functionality. Proof-of-concept experiments in the context of chemical and biosensing suggest that they may be useful for such applications, provided adequate levels of sensitivity can be demonstrated, especially with respect to biological analytes. Future efforts will be aimed at optimizing sensitivity and developing molecular printing technologies for aligning and integrating NBWs into macroscopic length scale devices.[44−48]

■ ASSOCIATED CONTENT

Ⓢ Supporting Information

Supplementary methods and additional details on the fabrication method, and supplementary figures. This material is available free of charge via the Internet at http://pubs.acs.org.

■ AUTHOR INFORMATION

Corresponding Author

*E-mail: seunghun@snu.ac.kr; chadnano@northwestern.edu

dx.doi.org/10.1021/nl204259t | *Nano Lett.* 2012, 12, 1879−1884

Author Contributions

[#]These authors contributed equally.

Notes

The authors declare no competing financial interest.

■ ACKNOWLEDGMENTS

This work was supported by the International Research & Development Program from the MEST (no. 2011-00240) and partly by the National Research Foundation grant (no. 2011-0000390). S.H. acknowledges the support from the Converging Research Center Program (no. 2011K000683) and the Public welfare and Safety research program (no. 20110020984) from the MEST. C.A.M. acknowledges the Asian Office of Aerospace Research and Development (AOARD) for support of this research. A.L.S. acknowledges the Electrochemical Society's 2011 Edward G. Weston Summer Research Fellowship.

■ REFERENCES

(1) Baughman, R. H.; Zakhidov, A. A.; de Heer, W. A. *Science* **2002**, *297*, 787−792.
(2) Javey, A.; Qi, P.; Wang, Q.; Dai, H. *Proc. Natl. Acad. Sci. U.S.A.* **2004**, *101*, 13408−13410.
(3) Javey, A.; Guo, J.; Paulsson, M.; Wang, Q.; Mann, D.; Lundstrom, M.; Dai, H. *Phys. Rev. Lett.* **2004**, *92*, 106804.
(4) Javey, A.; Guo, J.; Wang, Q.; Lundstrom, M.; Dai, H. *Nature* **2003**, *424*, 654−657.
(5) Mann, D.; Javey, A.; Kong, J.; Wang, Q.; Dai, H. *Nano Lett.* **2003**, *3*, 1541−1544.
(6) Guo, J.; Kan, E. C.; Ganguly, U.; Zhang, Y. *J. Appl. Phys.* **2006**, *99*, 084301.
(7) Heller, I.; Janssens, A. M.; Mannik, J.; Minot, E. D.; Lemay, S. G.; Dekker, C. *Nano Lett.* **2008**, *8*, 591−595.
(8) Kaul, A. B.; Wong, E. W.; Epp, L.; Hunt, B. D. *Nano Lett.* **2006**, *6*, 942−947.
(9) Brintlinger, T.; Fuhrer, M. S.; Melngailis, J.; Utke, I.; Bret, T.; Perentes, A.; Hoffmann, P.; Abourida, M.; Doppelt, P. *J. Vac. Sci. Technol. B* **2005**, *23*, 3174−3177.
(10) Qin, L.; Park, S.; Huang, L.; Mirkin, C. A. *Science* **2005**, *309*, 113−115.
(11) Qin, L.; Jang, J.-W.; Huang, L.; Mirkin, C. A. *Small* **2007**, *3*, 86−90.
(12) Osberg, K. D.; Schmucker, A. L.; Senesi, A. J.; Mirkin, C. A. *Nano Lett.* **2011**, *11*, 820−824.
(13) Qin, L.; Zou, S.; Xue, C.; Atkinson, A.; Schatz, G. C.; Mirkin, C. A. *Proc. Natl. Acad. Sci. U.S.A.* **2006**, *103*, 13300−13303.
(14) Qin, L.; Banholzer, M. J.; Millstone, J. E.; Mirkin, C. A. *Nano Lett.* **2007**, *7*, 3849−3853.
(15) Wei, W.; Li, S.; Millstone, J. E.; Banholzer, M. J.; Chen, X.; Xu, X.; Schatz, G. C.; Mirkin, C. A. *Angew. Chem., Int. Ed.* **2009**, *48*, 4210−4212.
(16) Wei, W.; Li, S.; Qin, L.; Xue, C.; Millstone, J. E.; Xu, X.; Schatz, G. C.; Mirkin, C. A. *Nano Lett.* **2008**, *8*, 3446−3449.
(17) Banholzer, M. J.; Osberg, K. D.; Li, S.; Mangelson, B. F.; Schatz, G. C.; Mirkin, C. A. *ACS Nano* **2010**, *4*, 5446−5452.
(18) Chen, X.; Jeon, Y.-M.; Jang, J.-W.; Qin, L.; Huo, F.; Wei, W.; Mirkin, C. A. *J. Am. Chem. Soc.* **2008**, *130*, 8166−8168.
(19) Chen, X.; Yeganeh, S.; Qin, L.; Li, S.; Xue, C.; Braunschweig, A. B.; Schatz, G. C.; Ratner, M. A.; Mirkin, C. A. *Nano Lett.* **2009**, *9*, 3974−3979.
(20) Chen, X.; Braunschweig, A. B.; Wiester, M. J.; Yeganeh, S.; Ratner, M. A.; Mirkin, C. A. *Angew. Chem., Int. Ed.* **2009**, *48*, 5178−5181.
(21) Banholzer, M. J.; Qin, L.; Millstone, J. E.; Osberg, K. D.; Mirkin, C. A. *Nat. Protoc.* **2009**, *4*, 838−848.
(22) Lee, M.; Im, J.; Lee, B. Y.; Myung, S.; Kang, J.; Huang, L.; Kwon, Y.-K.; Hong, S. *Nat. Nanotechnol.* **2006**, *1*, 66−71.
(23) Bak, J. H.; Kim, Y. D.; Hong, S. S.; Lee, B. Y.; Lee, S. R.; Jang, J. H.; Kim, M.; Char, K.; Hong, S.; Park, Y. D. *Nat. Mater.* **2008**, *7*, 459−463.
(24) Okamoto, F. *Jpn. J. Appl. Phys.* **1974**, *13*, 383−384.
(25) Kim, K. S.; Zhao, Y.; Jang, H.; Lee, S. Y.; Kim, J. M.; Kim, K. S.; Ahn, J.-H.; Kim, P.; Choi, J.-Y.; Hong, B. H. *Nature* **2009**, *457*, 706−710.
(26) Lim, D.-K.; Jeon, K.-S.; Kim, H. M.; Nam, J.-M.; Suh, Y. D. *Nat. Mater.* **2010**, *9*, 60−67.
(27) Lim, D.-K.; Jeon, K.-S.; Hwang, J.-H.; Kim, H.; Kwon, S.; Suh, Y. D.; Nam, J.-M. *Nat. Nanotechnol.* **2011**, *6*, 452−460.
(28) Homma, Y.; Chiashi, S.; Kobayashi, Y. *Rep. Prog. Phys.* **2009**, *72*, 066502−066523.
(29) Ventura, D. N.; Stone, R. A.; Chen, K.-S.; Hariri, H. H.; Riddle, K. A.; Fellers, T. J.; Yun, C. S.; Strouse, G. F.; Kroto, H. W.; Acquah, S. F.A. *Carbon* **2010**, *78*, 987−994.
(30) Dragoman, D.; Dragoman, M. *Phys. Rev. B* **2006**, *73*, 125417−125420.
(31) Suehiro, J.; Zhou, G.; Imakiire, H.; Ding, W.; Hara, M. *Sens. Actuators, B* **2005**, *108*, 398−403.
(32) Lee, H.; Lee, M.; Namgung, S.; Hong, S. *ACS Nano* **2010**, *4*, 7612−7618.
(33) Zhang, Z. Y.; Wang, S.; Ding, L.; Liang, X. L.; Xu, H. L.; Shen, J.; Chen, Q.; Cui, R. L.; Li, Y.; Peng, L.-M. *Appl. Phys. Lett.* **2008**, *92*, 133117.
(34) Franklin, A. D.; Chen, Z. *Nat. Nanotechnol.* **2010**, *5*, 858−862.
(35) Kong, J.; Franklin, N. R.; Zhou, C.; Chapline, M. G.; Peng, S.; Cho, K.; Dai, H. *Science* **2000**, *287*, 622−625.
(36) Maeng, S.; Moon, S.; Kim, S.; Lee, H.-Y.; Park, S.-J.; Kwak, J.-H.; Park, K.-H.; Park, J.; Choi, Y.; Udrea, F.; Milne, W. I.; Lee, B. Y.; Lee, M.; Hong, S. *Appl. Phys. Lett.* **2008**, *93*, 113111.
(37) Rosi, N. L.; Mirkin, C. A. *Chem. Rev.* **2005**, *105*, 1547.
(38) Taton, T. A.; Mirkin, C. A.; Letsinger, R. L. *Science* **2000**, *289*, 1757.
(39) Storhoff, J. J.; Elghanian, R.; Mucic, R. C.; Mirkin, C. A.; Letsinger, R. L. *J. Am. Chem. Soc.* **1998**, *120*, 1959.
(40) Lee, J. S.; Lytton-Jean, A. K. R.; Hurst, S. J.; Mirkin, C. A. *Nano Lett.* **2007**, *7*, 2112.
(41) Lee, S. W.; Lee, D. S.; Yu, H. Y.; Campbell, E. E. B.; Park, Y. W. *Appl. Phys. A: Mater. Sci. Process.* **2004**, *78*, 283−286.
(42) Sangwan, V. K.; Behnam, A.; Ballarotto, V. W.; Fuhrer, M. S.; Ural, A.; Williams, E. D. *Appl. Phys. Lett.* **2010**, *97*, 043111−043113.
(43) Byon, H. R.; Choi, H. C. *J. Am. Chem. Soc.* **2006**, *128*, 2188−2189.
(44) Piner, R. D.; Zhu, J.; Xu, F.; Hong, S.; Mirkin, C. A. *Science* **1999**, *283*, 661.
(45) Huo, F.; Zheng, Z.; Zheng, G.; Giam, L. R.; Zhang, H.; Mirkin, C. A. *Science* **2008**, *321*, 1658.
(46) Shim, W.; A. Braunschweig, B.; Liao, X.; Chai, J.; Lim, J. K.; Zheng, G.; Mirkin, C. A. *Nature* **2011**, *469*, 516.
(47) Braunschweig, A. B.; Huo, F.; Mirkin, C. A. *Nat. Chem.* **2009**, *1*, 353.
(48) Giam, L. R.; Mirkin, C. A. *Angew. Chem., Int. Ed.* **2011**, *50*, 7482.